Supporting Information

Disparate Redox Potentials in Mixed Isomer Electrolytes Reduce Voltage Efficiency of Energy Dense Flow Batteries

Casey M. Davis [1], Scott E. Waters [1], Brian H. Robb [2], Jonathan R. Thurston [1], David Reber [3,*] and Michael P. Marshak [1,4]

[1] Department of Chemistry, University of Colorado Boulder, Boulder, CO 80309, USA; jonathan.thurston@colorado.edu (J.R.T.)
[2] Department of Chemical and Biological Engineering, University of Colorado Boulder, Boulder, CO 80309, USA
[3] Empa, Swiss Federal Laboratories for Materials Science and Technology, 8600 Dübendorf, Switzerland
[4] Renewable and Sustainable Energy Institute, University of Colorado Boulder, Boulder, CO 80309, USA
* Correspondence: david.reber@empa.ch

Table of Contents

I. CHARACTERIZATION

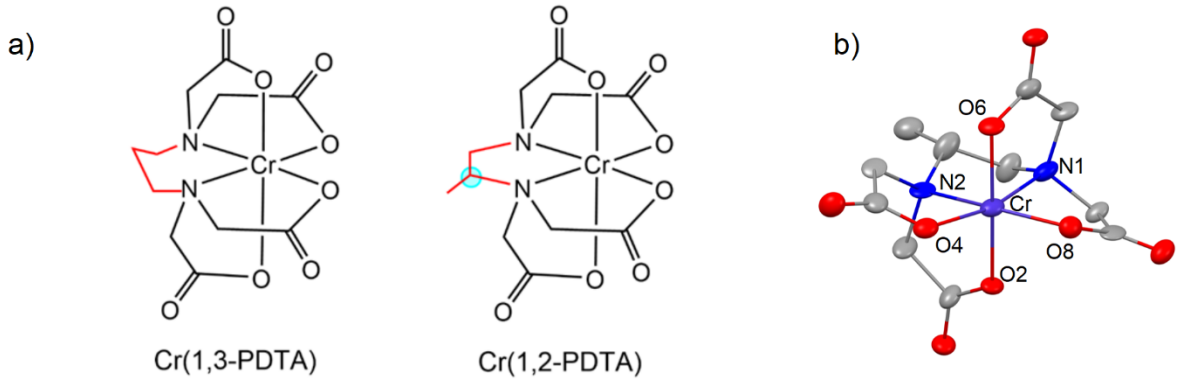

Figure S1. Representations of the monoanionic structurally isomeric chromium-chelate complexes. a) Cr(1,3-PDTA) and Cr(1,2-PDTA) with the stereocenter highlighted in blue and b) the single-crystal X-ray diffraction structure of Cr(1,2-PDTA) with hydrogens, potassium, and waters omitted for clarity, showing 50% probability thermal ellipsoids. Analysis is qualitative as the enantiomeric nature of KCr(1,2-PDTA) prevented the acquisition of high-quality data.

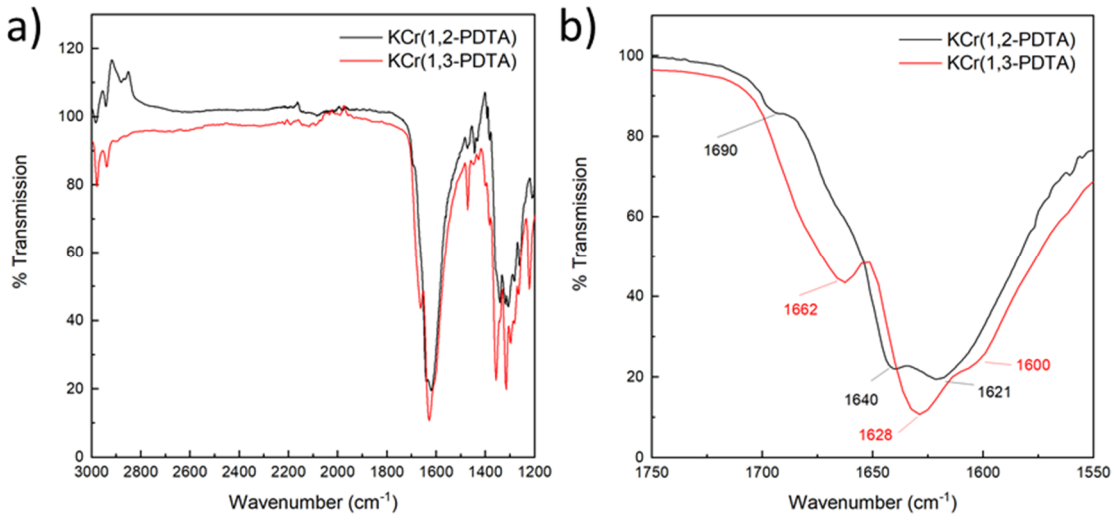

Figure S2. IR spectroscopy data of the examined Cr(1,2-PDTA) and Cr(1,3-PDTA) complexes. a) full spectrum, b) C=O stretching region.

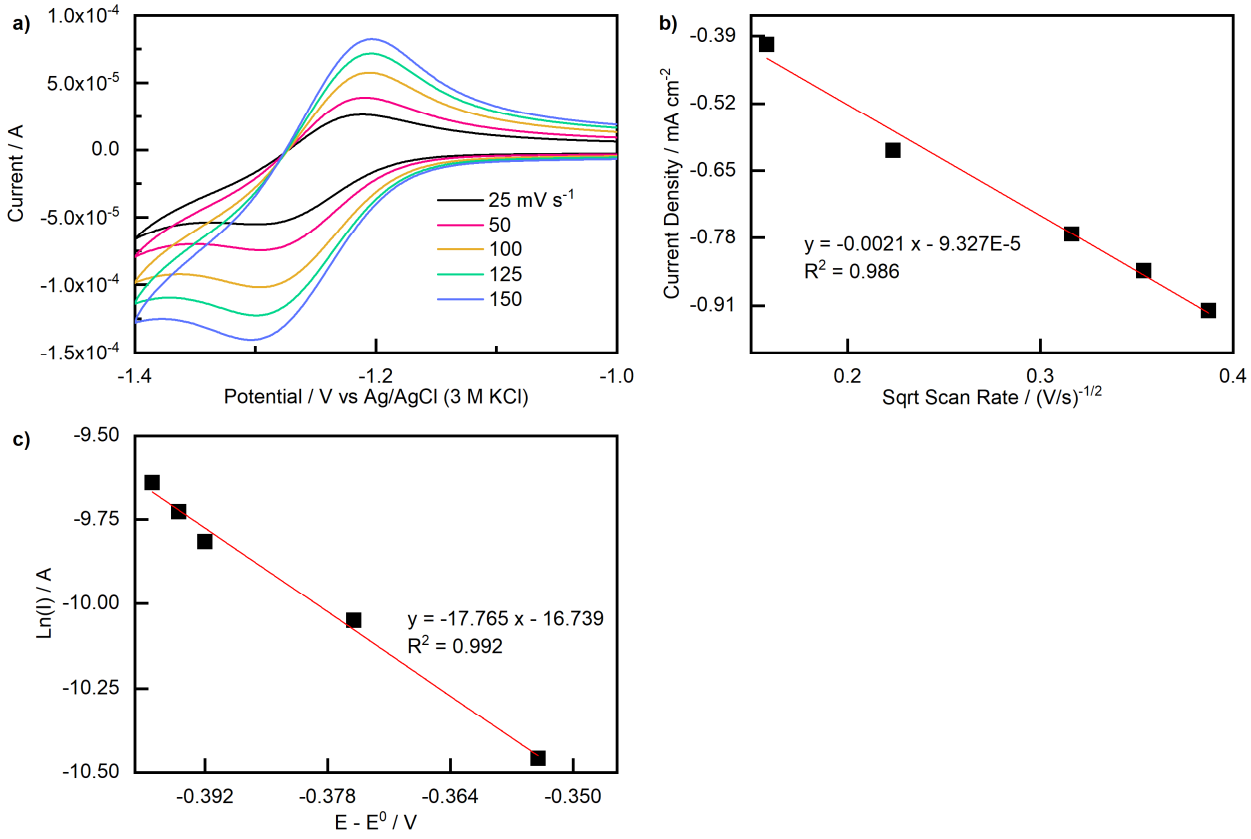

Figure S3. Cyclic voltammetry of 5 mM KCr(1,2-PDTA) in 0.5 M KCl and 0.1 M 1,2-PDTA at pH 7.05 for electrochemical kinetic studies. (a) Cyclic voltammograms at varying scan rates. (b) Peak reduction current density as a function of the square root of the scan rate, $v^{1/2}$. (c) The natural log of the peak reduction current (i_{pc}) as a function of the difference in potential between calculated E^0 and the voltage at the peak reduction current density (E_{pc}).

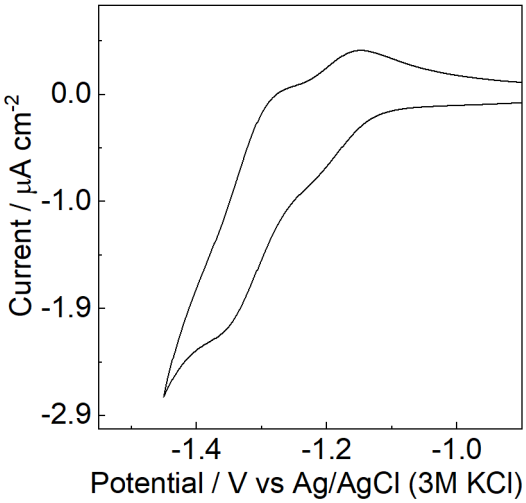

Figure S4. Cyclic voltammetry of 10 mM total equimolar mixed KCr(1,2-PDTA) and KCr(1,3-PDTA) at pH 7 on a bismuth-functionalized glassy carbon electrode.

II. FLOW BATTERY CELL DATA

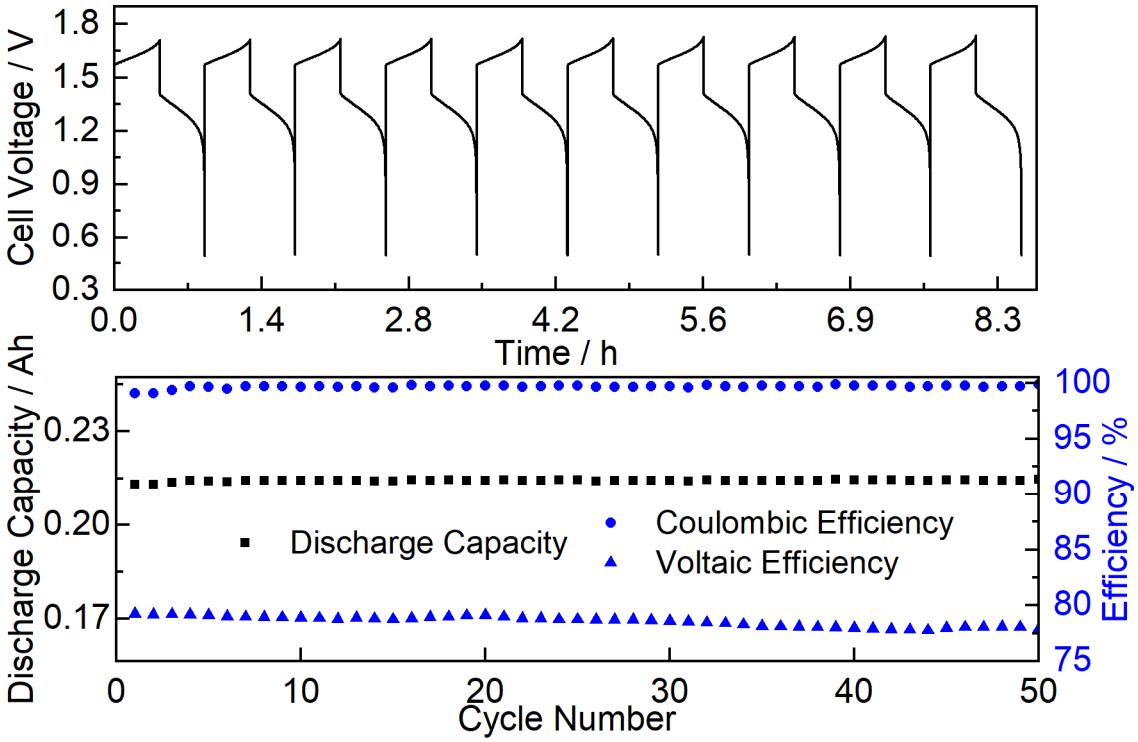

Figure S5. Redox flow battery (RFB) cell cycling data of 1 M KCr(1,2-PDTA) versus HCF. (Top) Cell voltage as a function of time for the first ten cycles. (Bottom) Discharge capacity and voltage and Coulombic efficiencies over the 50 cycles.

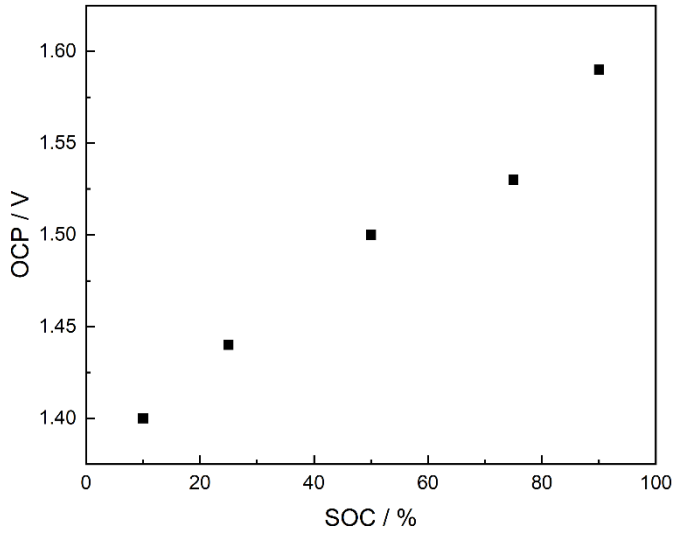

Figure S6. Open circuit potential vs. state-of-charge of the negolyte for 1 M KCr(1,2-PDTA).

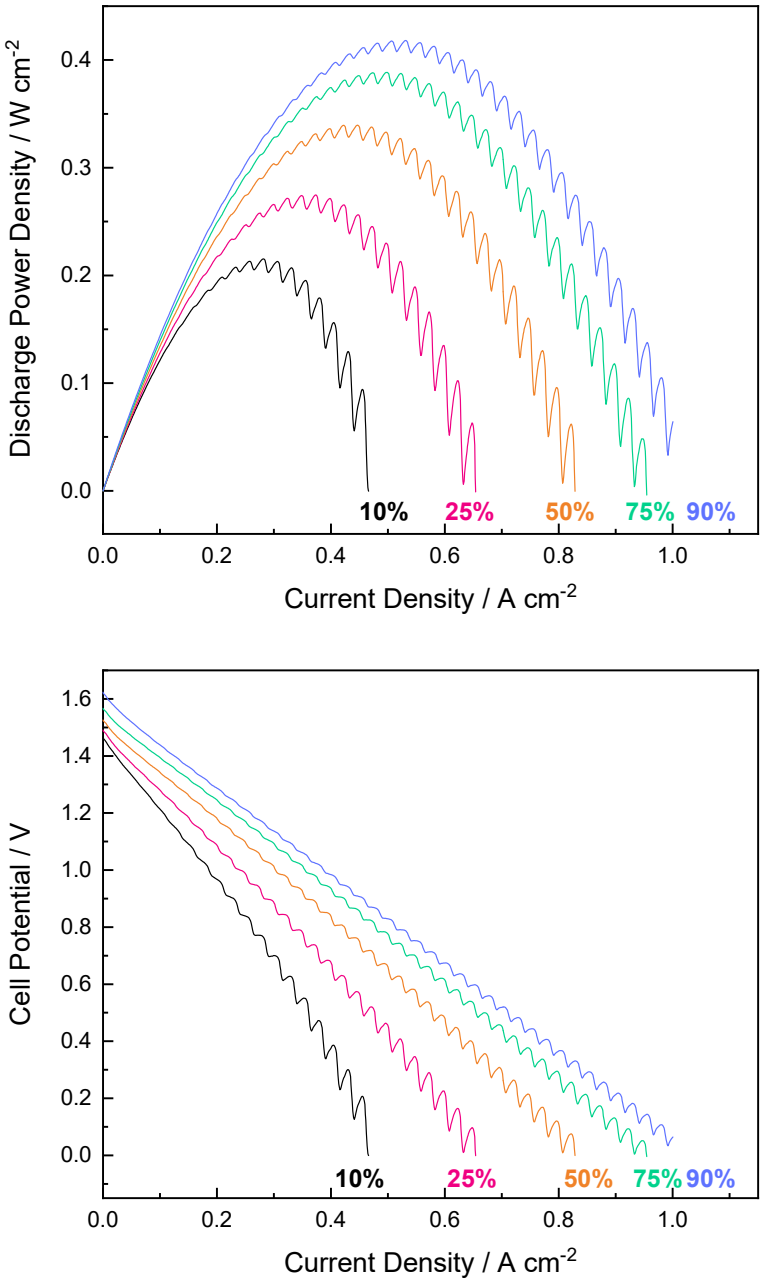

Figure S7. Power data for the 1 M KCr(1,2-PDTA) cell. (Top) Discharge power density as a function of current density. (Bottom) Polarization curves demonstrating cell potential as a function of current density. The pulsing of the lines is caused by the pump action of the peristaltic pumps.

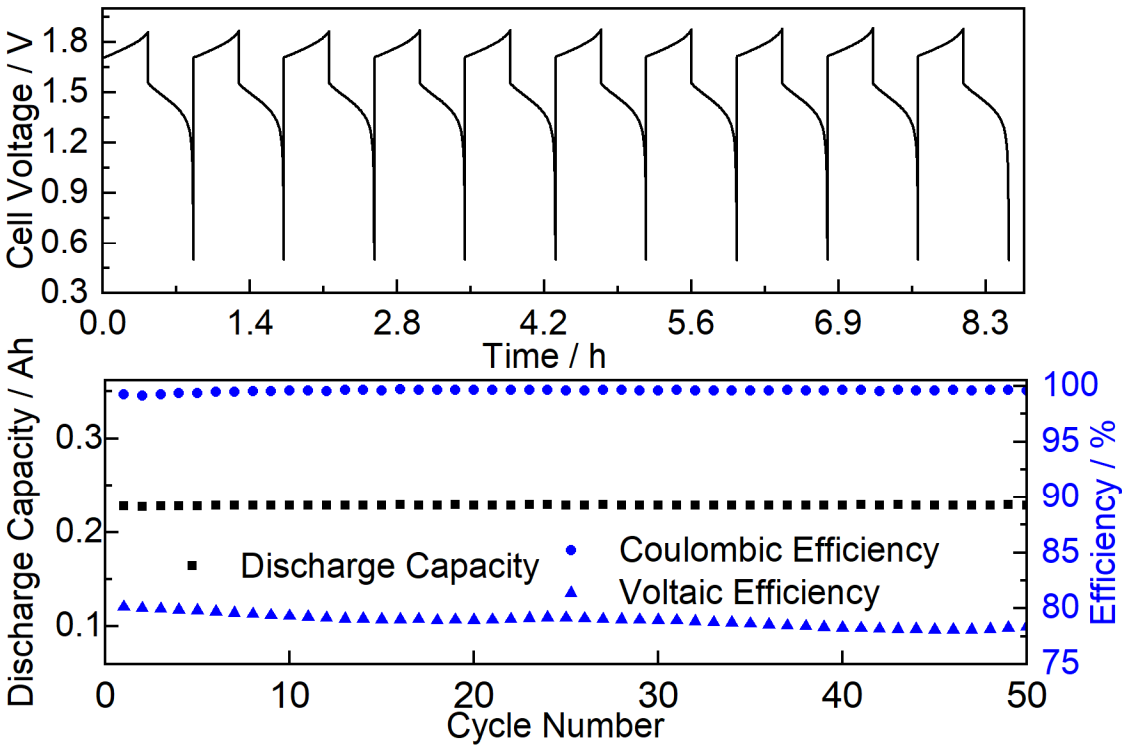

Figure S8. RFB cell cycling data of 1 M KCr(1,3-PDTA) versus HCF. (Top) Cell voltage as a function of time for the first ten cycles. (Bottom) Discharge capacity and voltage and Coulombic efficiencies over the 50 cycles.

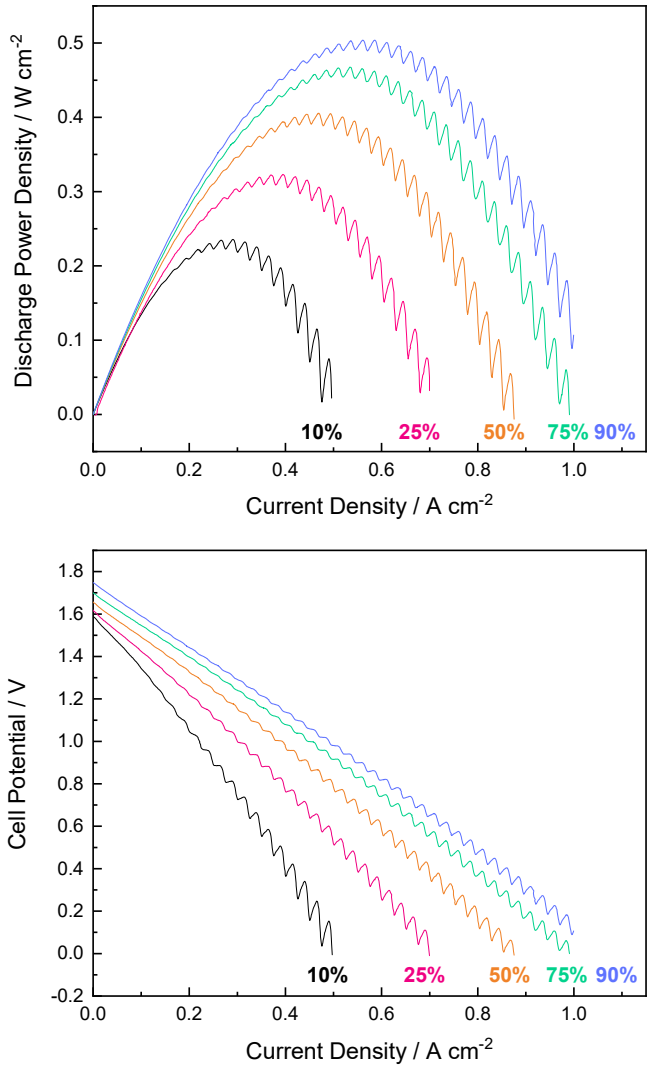

Figure S9. Power data for the 1 M KCr(1,3-PDTA) cell. (Top) Discharge power density as a function of current density. (Bottom) Polarization curves demonstrating cell potential as a function of current density.

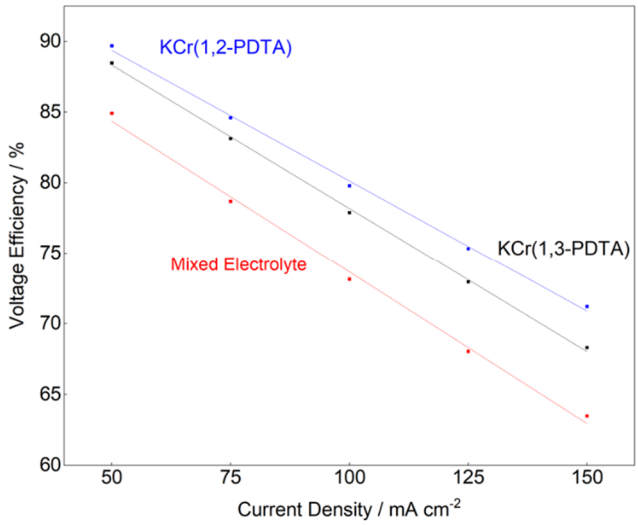

Figure S10. Voltage efficiency vs. current density for the 1 M KCr(1,2-PDTA), 1 M KCr(1,3-PDTA), and mixed 1 M cells.

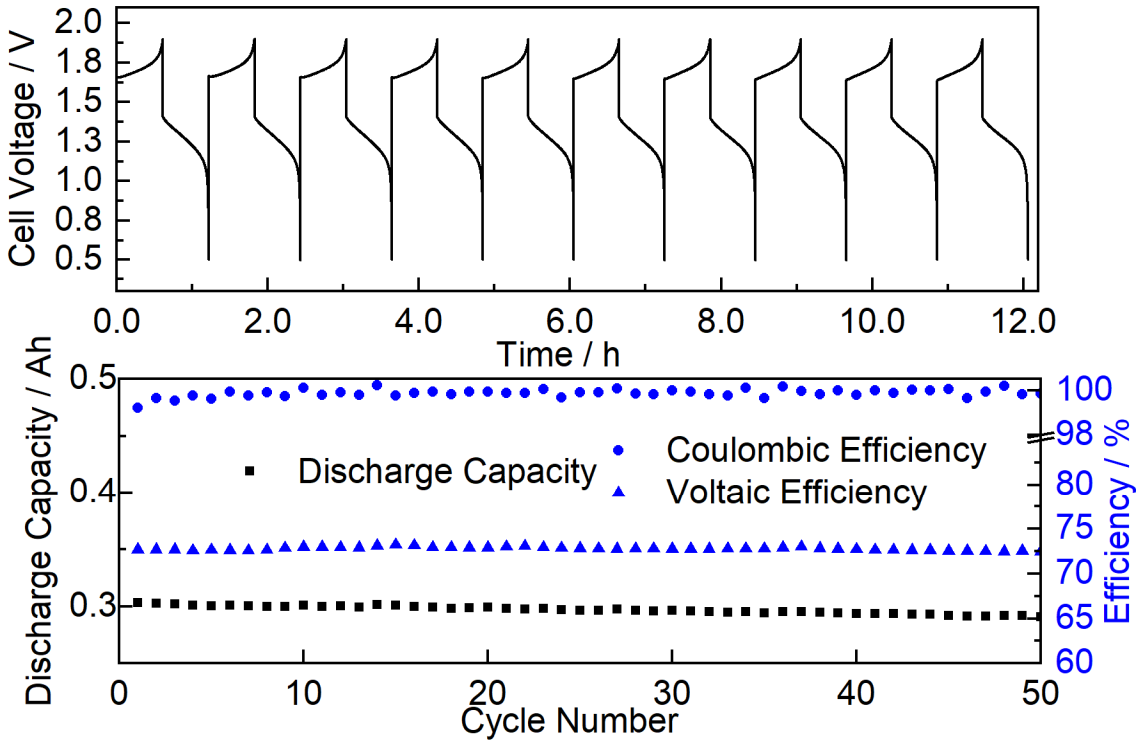

Figure S11. RFB cell cycling data of 1.5 M KCr(1,2-PDTA) versus HCF. (Top) Cell voltage as a function of time for the first ten cycles. (Bottom) Discharge capacity and voltage and Coulombic efficiencies across the 50 cycles.

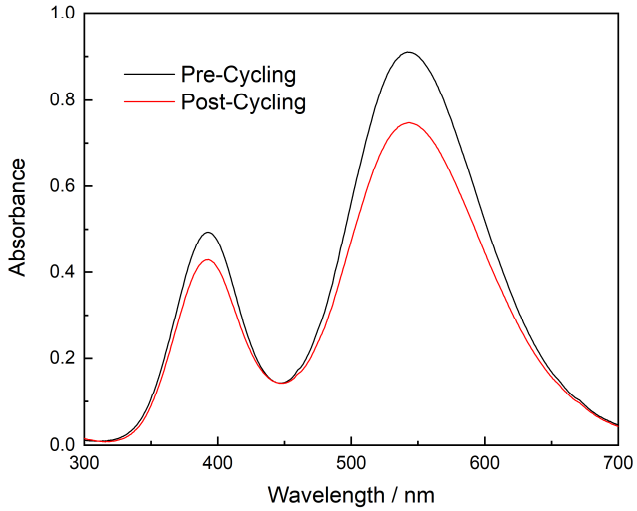

Figure S12. UV-Vis spectra of 0.1 M KCr(1,2-PDTA) with 0.1 M 1,3-PDTA buffer electrolyte bulk electrolyzed to test for ligand exchange.

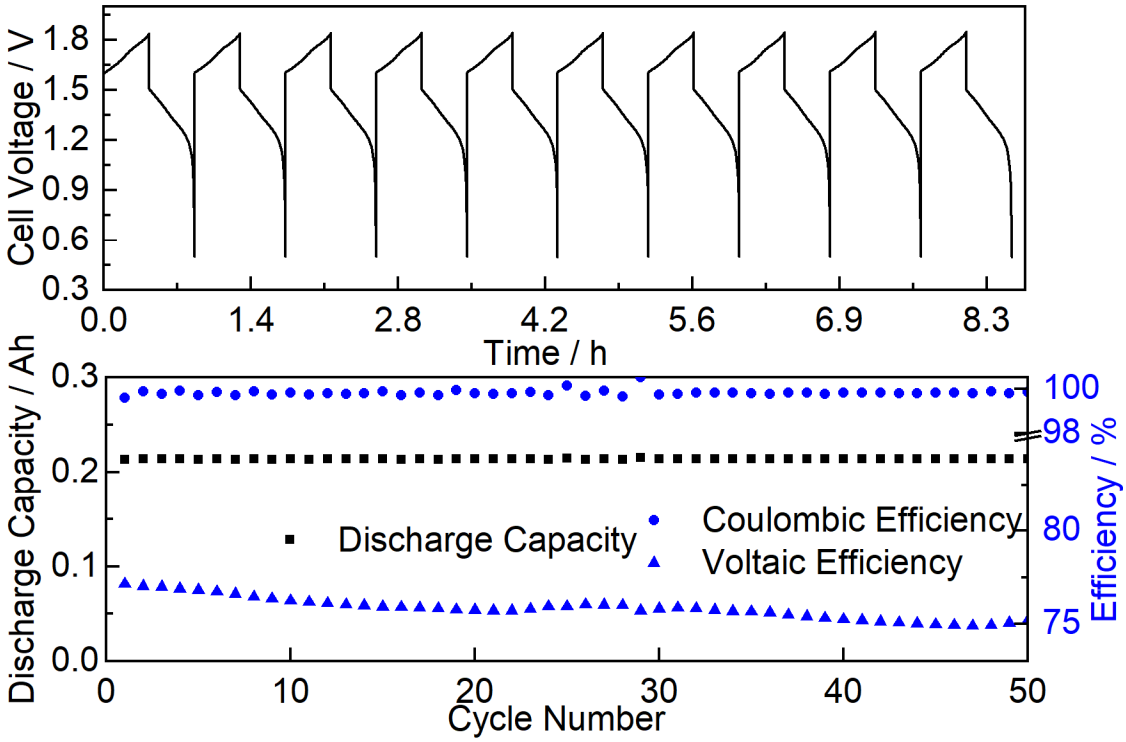

Figure S13. RFB cell cycling data of the mixed electrolyte cell with a total 1 M Cr negolyte comprising 0.5 M KCr(1,2-PDTA) and 0.5 M KCr(1,3-PDTA) versus HCF. Cell voltage as a function of time for the first ten cycles. (Bottom) Discharge capacity and voltage and Coulombic efficiencies across the 50 cycles.

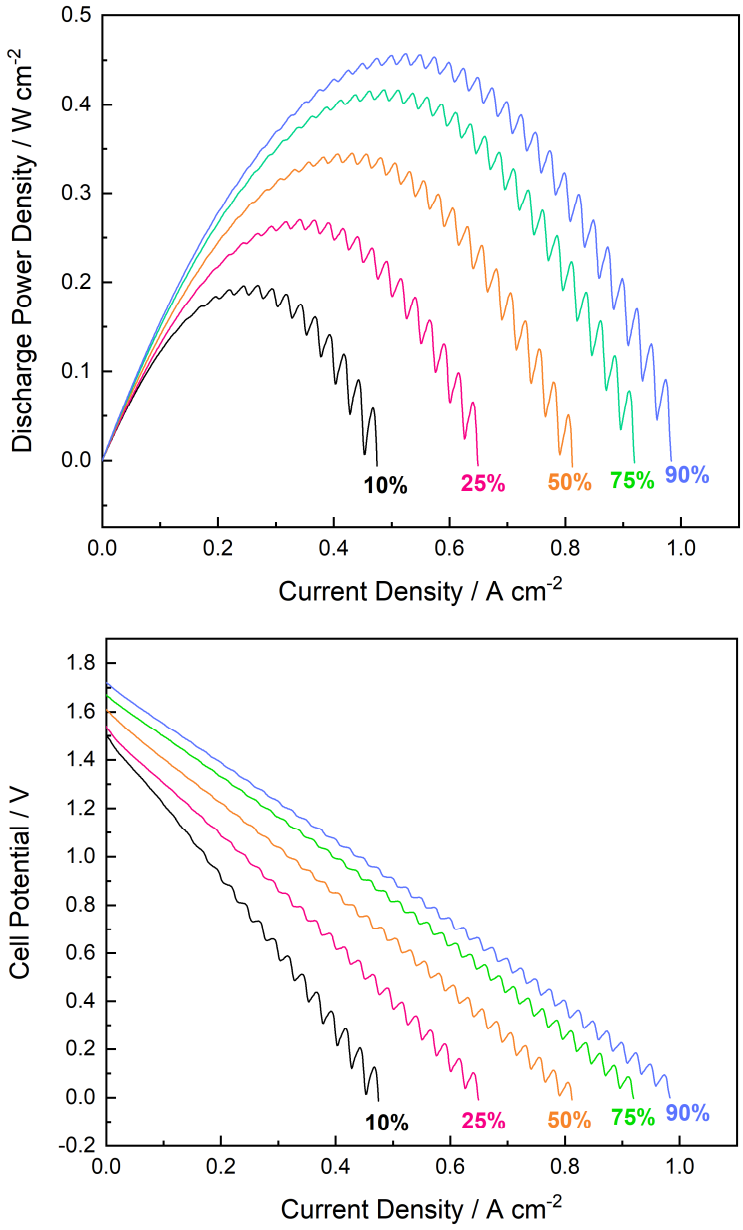

Figure S14. Power data for the mixed electrolyte cell with a total 1 M Cr negolyte comprising 0.5 M KCr(1,2-PDTA) and 0.5 M KCr(1,3-PDTA) versus HCF. (Top) Discharge power density as a function of current density. (Bottom) Polarization curves demonstrating cell potential as a function of current density.

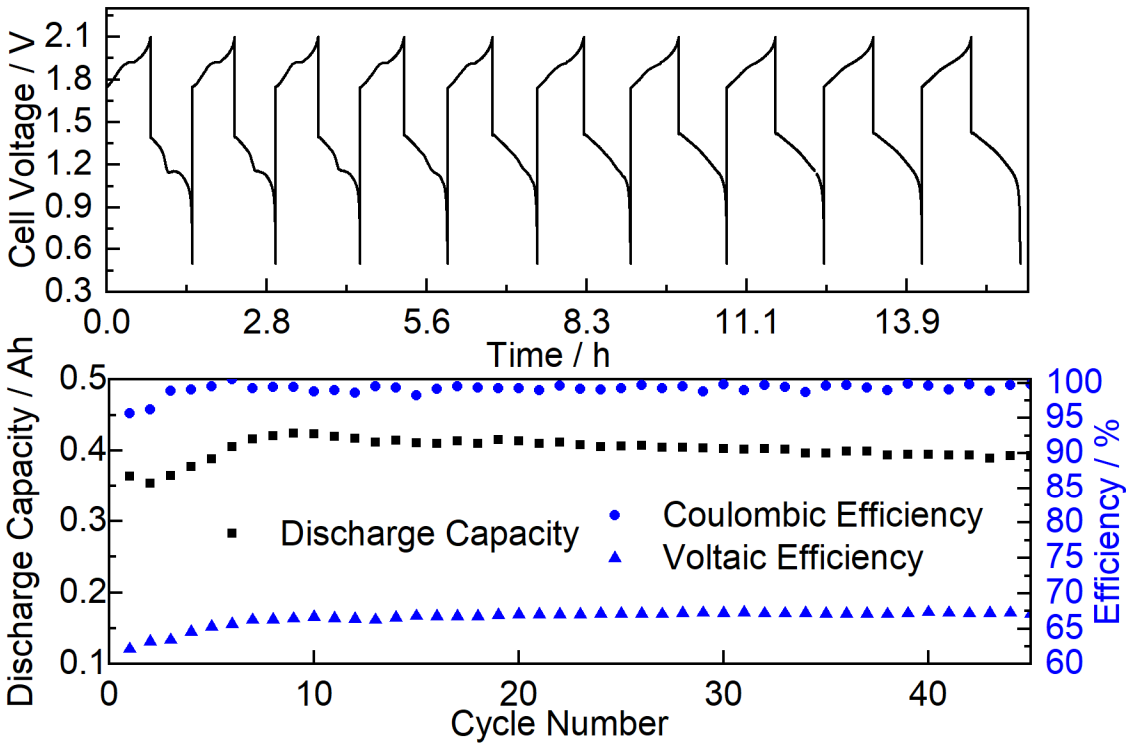

Figure S15. RFB cell cycling data of the mixed electrolyte cell with a total 2 M Cr negolyte comprising 1 M KCr(1,2-PDTA) and 1 M KCr(1,3-PDTA) versus HCF. (Top) Cell voltage as a function of time for the first ten cycles. (Bottom) Discharge capacity and voltage and Coulombic efficiencies across the 50 cycles.

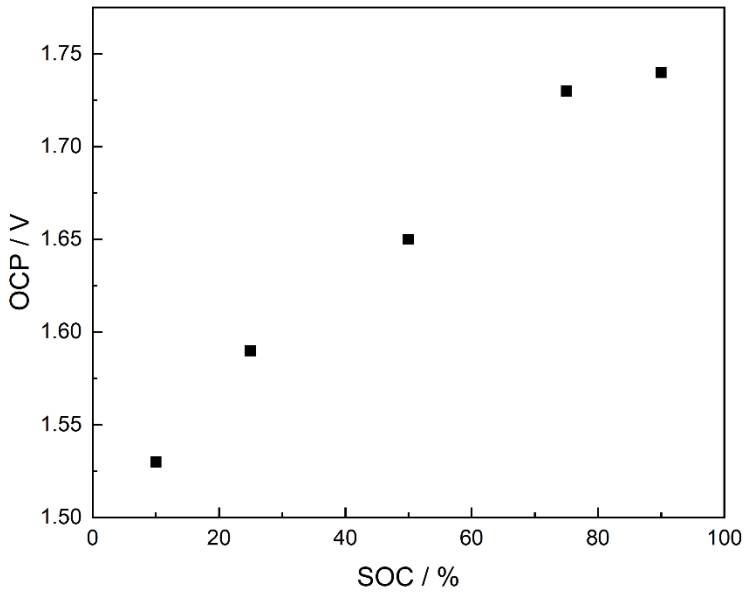

Figure S16. Open circuit potential as a function of state-of-charge of the cell containing the 2 M mixed negolyte.

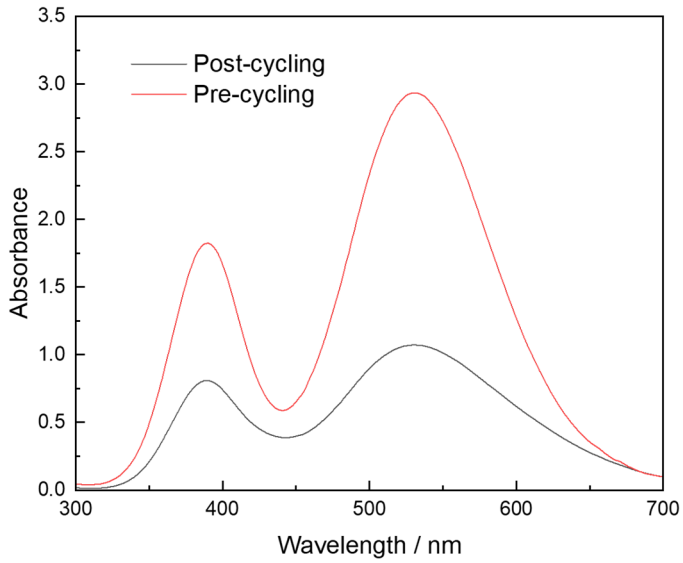

Figure S17. UV-Vis analysis of 2 M cell before and after cycling.

III. TABLES AND EQUATIONS

Table S1. X-ray Crystallographic Table for KCr(1,2-PDTA).

	2
Formula	$KCrN_2O_8H_{14}C_{11}$
fw, g/mol	437.367
Temperature	100(2) K
cryst. syst.	Monoclinic
space group	P 1 21/c 1
color	Dark Violet
a (Å)	19.410(3)
b (Å)	13.474(2)
c (Å)	13.4160(16)
α (deg)	90
β (deg)	104.775(6)
γ (deg)	90
V (Å^3)	3392.7(8)
Z	8
no. refl.	43130
unique refl.	6665
R_{int}	0.1690
R1[a] (all data)	0.1690
*w*R2[b] (all data)	0.1168
R1 [(I > 2σ)]	0.0889
*w*R2 [I > 2σ)]	0.0978
GOF[c]	1.0828

[a] $R1 = \Sigma||F_o| - |F_c||/\Sigma|F_o|$. [b] $wR2 = (\Sigma(w(F_o^2 - F_c^2)^2)/\Sigma(w(F_o^2)^2))^{1/2}$. [c] $GOF = (\Sigma\, w(F_o^2 - F_c^2)^2/(n - p))^{1/2}$ where *n* is the number of data and *p* is the number of parameters refined.

Table S2. IR peaks of each complex in the C=O stretching region (1690-1600 cm^{-1}).

	Peak 1 / cm^{-1}	**Peak 2 / cm^{-1}**	**Peak 3 / cm^{-1}**
KCr(1,2-PDTA)	1690	1640	1621
KCr(1,3-PDTA)	1662	1628	1600

Table S3. UV-Vis peaks and respective molar absorptivities for KCr(1,2-PDTA) and KCr(1,3-PDTA).

	Peak 1 (nm) / molar absorptivity (M^{-1} cm^{-1})	**Peak 2 (nm) / molar absorptivity (M^{-1} cm^{-1})**
KCr(1,2-PDTA)	391 / 105	541 / 191
KCr(1,3-PDTA)	382 / 83	506 / 116

Table S4. Heterogeneous rate transfer constants (k^0) and diffusion coefficients (D_o) of KCr(1,2-PDTA) and KCr(1,3-PDTA).[1]

	Heterogeneous Electron Transfer Rate k^0 ($x10^{-4}$ cm s^{-1})	Diffusion Coefficient D_o ($x\ 10^{-6}$ cm^2 s^{-1})
KCr(1,2-PDTA)	1.1	4.1
KCr(1,3-PDTA)	1.7	6.2

Table S5. Relevant electrolyte densities, viscosities, and area specific resistances (ASRs).

	Density (g/ml)	Viscosity (cP)	ASR (Ω cm^2)
1 M KCr(1,2-PDTA)	1.1	1.4	1.6
1 M KCr(1,3-PDTA)	1.2[2]	2.2[2]	1.7
2 M Mixed	1.4	5.5	3.37

Equation S1. Relationship of reduction potential with binding constant for Cr(III)/Cr(II)[3]:

$$E^{0\prime} = E^{0\prime}_{Cr^{3+}+Cr^{2+}} + \frac{RT}{F}\ln\left(\frac{KCr_{IIILn}}{KCr_{IIILn}}\right)$$

IV. REFERENCES

(1) Robb, B. H.; Farrell, J. M.; Marshak, M. P. Chelated Chromium Electrolyte Enabling High-Voltage Aqueous Flow Batteries. *Joule* **2019**, *3* (10), 2503–2512. https://doi.org/10.1016/j.joule.2019.07.002.

(2) Reber, D.; Thurston, J. R.; Becker, M.; Pach, G. F.; Wagoner, M. E.; Robb, B. H.; Waters, S. E.; Marshak, M. P. Mediating Anion-Cation Interactions to Improve Aqueous Flow Battery Electrolytes. *Appl. Mater. Today* **2022**, *28*, 101512. https://doi.org/10.1016/j.apmt.2022.101512.

(3) Robb, B. H.; Waters, S. E.; Marshak, M. P. Evaluating Aqueous Flow Battery Electrolytes: A Coordinated Approach. *Dalton Trans.* **2020**, *49* (45), 16047–16053. https://doi.org/10.1039/D0DT02462G.